PHYSICAL REVIEW E **84**, 060901(R) (2011)

# Electronic properties of conductive pili of the metal-reducing bacterium *Geobacter sulfurreducens* probed by scanning tunneling microscopy

Joshua P. Veazey,[1] Gemma Reguera,[2,*] and Stuart H. Tessmer[1,†]

[1]*Department of Physics & Astronomy, Michigan State University, East Lansing, Michigan 48824-2320, USA*

[2]*Department of Microbiology & Molecular Genetics, Michigan State University, East Lansing, Michigan 48824-4320, USA*

(Received 12 August 2011; published 6 December 2011)

The metal-reducing bacterium *Geobacter sulfurreducens* produces conductive protein appendages known as "pilus nanowires" to transfer electrons to metal oxides and to other cells. These processes can be harnessed for the bioremediation of toxic metals and the generation of electricity in bioelectrochemical cells. Key to these applications is a detailed understanding of how these nanostructures conduct electrons. However, to the best of our knowledge, their mechanism of electron transport is not known. We used the capability of scanning tunneling microscopy (STM) to probe conductive materials with higher spatial resolution than other scanning probe methods to gain insights into the transversal electronic behavior of native, cell-anchored pili. Despite the presence of insulating cellular components, the STM topography resolved electronic molecular substructures with periodicities similar to those reported for the pilus shaft. STM spectroscopy revealed electronic states near the Fermi level, consistent with a conducting material, but did not reveal electronic states expected for cytochromes. Furthermore, the transversal conductance was asymmetric, as previously reported for assemblies of helical peptides. Our results thus indicate that the *Geobacter* pilus shaft has an intrinsic electronic structure that could play a role in charge transport.

DOI: 10.1103/PhysRevE.84.060901 PACS number(s): 87.15.−v, 87.64.Dz

Dissimilatory metal-reducing bacteria in the family *Geobacteraceae* gain energy for growth by transferring metabolically generated electrons to external electron acceptors such as insoluble Fe(III) oxides, a process that could be harnessed for the bioremediation of soluble toxic metals and the production of electricity in bioelectrochemical cells. Extracellular electron transfer in these organisms requires the expression of conductive protein nanofilaments that are phylogenetically related to bacterial type IV pili [1]. In addition to being required for the reduction of Fe(III) oxides [1], the conductive pili also function as electronic conduits between cells in biofilms formed on Fe(III) oxide coatings [2] and in current-producing anode biofilms [3]. As with other pili, the *Geobacter* pili are formed through the polymerization of a single helical peptide subunit or pilin [1,4]. However, little is known about the mechanism that enables the pili to conduct electrons and the potential contribution of the pilus protein shaft to its conductivity.

The hybridization of antibodies raised against outer membrane *c*-cytochromes to pili-like filaments of the model organism *Geobacter sulfurreducens* raised the possibility that *c*-cytochromes assembled on the pili could play a role in electron transfer [5]. This interpretation contrasts with studies [6] suggesting that the pili, rather than cytochromes, were responsible for the conductivity detected in heterogeneous preparations of pili after heat treatment, which presumably denatured the cytochromes without affecting the pili. These previous studies are difficult to interpret because the biochemical nature of the pili samples was either never confirmed [5,6] and/or samples were processed by chemical fixation [5], heat treatment [6], or mechanical shearing [6], which are all treatments that can affect the biochemical structure and integrity of proteins and other cellular components and can mask the true contribution of the pili or cytochromes to the measured conductivity. Heat denaturation, for example, was used to denature the cytochromes present in heterogenous pili preparations [6]. However, these studies never assessed the effect of heat denaturation on pili stability and the potential doping of the samples resulting from the release of the cytochromes' metal contents after heat denaturation. Not surprisingly, the conductivity measured in these samples was metallic in nature [6].

These early studies highlighted the need to use direct, unbiased methods to investigate if the pilus shaft and/or cytochromes contribute to the pilus conductivity. If cytochromes are responsible for the pilus conductivity, this mechanism would be similar to that of the nanowires produced by the metal-reducing bacterium *Shewanella oneidensis* MR-1, which rely on outer membrane *c*-cytochromes aligned onto a filamentous scaffold to transfer electrons distally and axially [7,8]. Furthermore, transversal conductance measurements using a conductive probe atomic force microscope (CP-AFM) produced reproducible peaks for the cytochrome heme groups that corresponded to regions of the nanowires with higher density of states [9]. Similar transversal conductivity measurements of carbon nanotubes linking metalloproteins were interpreted in the context of long-distance linkage of metalloproteins to metal surfaces [10]. Thus, these studies demonstrated that it was possible to use scanning probe methods to directly detect cytochrome heme signatures on microbial nanowires and gain insights into their mechanism of conductivity.

Previous conductance measurements with a CP-AFM [1] demonstrated the transversal conductive nature of the pili produced by *G. sulfurreducens* but provided little information about their electronic properties. Furthermore, the pili were mechanically detached from the cell surface [1], which results in heterogeneous preparations composed of pili and other

*reguera@msu.edu
†tessmer@msu.edu

 

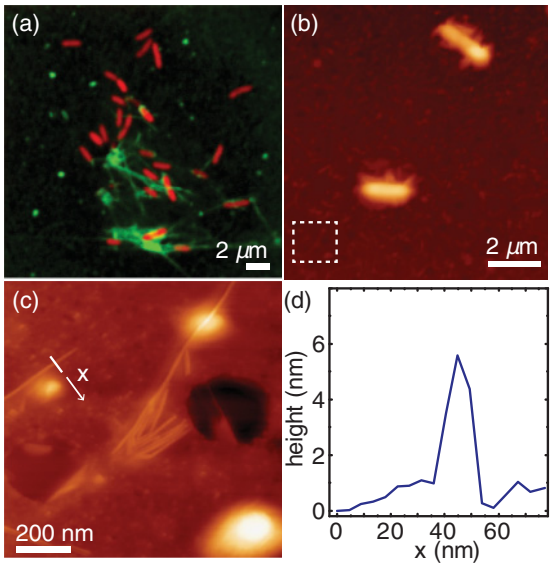


FIG. 1. (Color online) (a) Confocal scanning laser microscopy (CSLM) imaging of aggregates of cells (red/gray) with interconnecting pili (green/light gray). (b), (c) AFM image of pili-expressing cells deposited onto the surface of HOPG (b) and higher-resolution AFM topography of the region marked in (b) showing the pilus network within the cell aggregates (c). (d) Height profile of a pilus filament at the location marked in (c).

sheared outer membrane components, such as loosely bound outer membrane *c*-cytochromes [11] and uncharacterized insulating materials [1]. Thus, to prevent the nonspecific adsorption of other cell components to the pili, which can either insulate the pili from the tip [1] or produce artifactual electronic features [6], we directly probed the conductive pili produced by cells of *G. sulfurreducens*. Biological samples were prepared by growing *G. sulfurreducens* cells to late-exponential phase in a fresh water (FW) medium with acetate and fumarate under pili-expressing conditions (25 °C), as previously described [1]. The expression of the pili under these conditions promotes cell aggregation [2]. The cell aggregates, which contain cells interconnected with the conductive pili, were imaged with confocal laser scanning microscopy (CLSM) [Fig. 1(a)]. For this experiment, the cells were stained for 30 min with the DNA-binding red dye SYTO 63 (Invitrogen), whereas the pili were first hybridized for 1 h with rabbit anti-PilA antibodies [generated against the carboxy-terminus domain of the pilin subunit (PilA) of the conductive pili] and then incubated with an antirabbit secondary antibody conjugated with the green SYTO 9 dye (Invitrogen). The nanofilaments, but not the cells, hybridized with the anti-PilA antibodies [Fig. 1(a)]. This demonstrates that the abundant nanofilaments are the PilA-containing pili previously shown to be conductive by CP-AFM [1]. Furthermore, the antibodies hybridized well along the pili, suggesting that numerous pilin epitopes were exposed, as expected of pili samples that are mostly free of adsorbed materials and have substantial areas of the pilus shaft exposed. The cell aggregates were also adsorbed onto the surface of freshly cleaved highly oriented pyrolytic graphite (HOPG) for 10–15 min. The excess moisture was aspirated and gently wicked dry with absorbent paper. All steps were performed in an anaerobic glove bag (Coy Laboratories). The adsorbed sample was then imaged by AFM using a Dimension 3100 (Digital Instruments) scanning probe microscopy (SPM) in tapping mode equipped with silicon cantilevers having spring constants of 42 N/m (Bruker). AFM imaging revealed abundant pili interspersed with cells and some extracellular debris [Fig. 1(b)]. However, clean regions of the pilus filaments were easily spotted and produced heights (∼5 nm) consistent with the diameter of the pilus shaft [Figs. 1(c) and 1(d)].

Scanning tunneling microscopy (STM) was used to image the conductive pili, as it produces real-space images and electron energy spectra of conductive materials with higher spatial resolution than the CP-AFM technique used before [1]. The biological sample was adsorbed on HOPG as described above. Controls with chemically fixed samples (prepared as previously described [1]) or freshly cleaved, bare HOPG (lacking biological samples) were also examined. STM imaging was performed with a home-built Besocke design scan head [12] integrated with a high vacuum chamber [13], equipped with a commercial controller (RHK Technology), and operated in constant current mode. A voltage was applied to the sample while holding the tip at ground. Bias voltages and current set points are indicated in each figure caption. Following the placement of biological samples, the STM chamber was immediately pumped to high vacuum ($\sim 10^{-6}$ Torr) and the samples were probed with a mechanically cut Pt:Ir (85:15) tip. The dense pilus network in the sample increased the chances of locating the conductive pili with the STM tip. Furthermore, although STM requires a stable tunneling current for probing, which often limits its application to relatively pure conductive structures free of insulating debris, the presence of many clean regions in the pili facilitated their characterization on the HOPG substrate in STM topography scans. As shown in Fig. 2, the STM images revealed abundant conductive filaments. Pili were especially abundant in chemically fixed samples [Fig. 2(a)], suggesting that the chemical treatment also promoted the adsorption of pili to the HOPG surface. Pili were also imaged in samples that had not undergone any chemical treatment. The lack of chemical fixation revealed beadlike structural features along the filaments, which were ∼5–7 nm in diameter [Fig. 2(b)]. This is larger than the ranges (2–4 nm) previously measured by CP-AFM [1]. The apparent broadening could be the result of the geometric and electronic convolution of the STM tip with the filamentous pilus, which rises above the relatively flat HOPG surface. Broadening by as much as 50%–300% was reported for carbon nanotubes adsorbed onto HOPG and was directly proportional to the nanotube width, thus enabling an estimate of the true diameter of the filament [14]. Inasmuch as we used a similar STM tip as in these previous studies [14], we were able to estimate the contribution of the tip-induced convolution of the geometry and electronic structure of the pilus filament. Using this approach, we estimated actual pili diameters between 3 and 5 nm, consistent with the diameters measured by AFM [1].

We further investigated the electronic properties of the conductive pili in samples that had not been fixed chemically by imaging a region of the pilus shown in Fig. 2(b) while sweeping the applied voltage [Fig. 2(c)]. The intensity of the bright spots observed along the pilus filament changed with the voltage applied [Fig. 2(c)]. Furthermore, the imaging asymmetry was restored when the voltage was returned to the

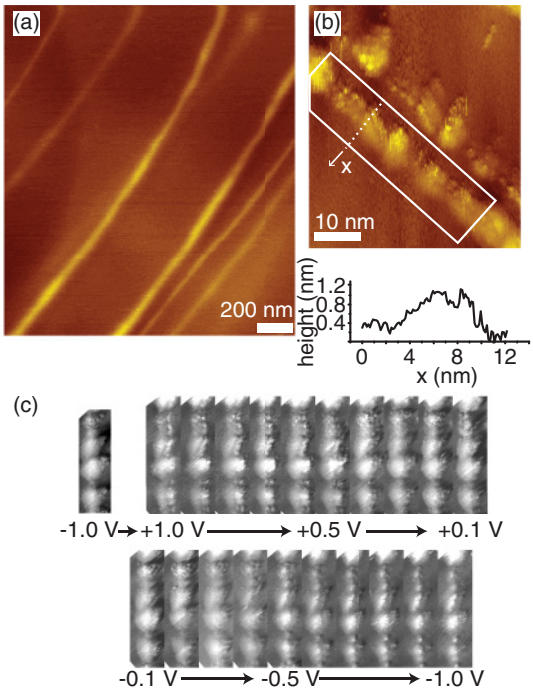


FIG. 2. (Color online) STM topography of conductive pili deposited on HOPG. (a) Chemically fixed samples showing pilus filaments and bundles of pili (thicker filaments) ($V = -500$ mV, $I =$ 63 pA). (b) Topographic image (top panel) and height measurements (bottom panel) of a pilus filament from air-dried samples. Height measurements were taken at the pilus location marked with a discontinuous line ($V = 0.9$ V, $I = 84$ pA). (c) Voltage-dependence (0.1-V increments) of the topographic features shown in the pilus region marked with a box in (b). The topographic structure was restored when we returned the voltage to $-1$ V after the sweep ($I =$ 60–85 pA).

initial value of $-1.0$ V [Fig. 2(c)], thus ruling out any damage to the STM tip upon repeated sweeps. This demonstrates that the contrast in the tunneling signal at these bright spots is caused in part by variations in the local density of states. This is consistent with these bright locations being molecular

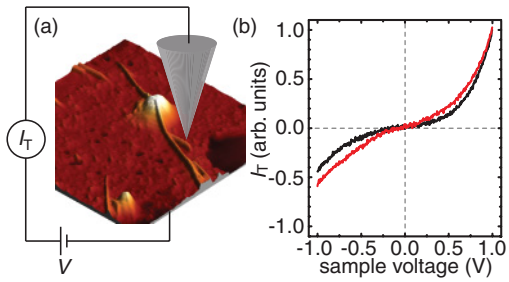


FIG. 3. (Color online) (a) Schematic of a typical STM spectroscopy measurement, with the STM tip positioned on a pilus filament deposited on HOPG. The voltage $V$ applied across the tip and sample is swept while the resulting tunneling current $I_T$ is read. Shown is an AFM topographic image of a pilus filament on HOPG. (b) Representative $I_T$-$V$ curve obtained for the pilus (red/gray) and the underlying graphite (black). The curves shown are averages of 1000 curves obtained consecutively on the same location.

substructures produced by "hot spots" of conductivity of the pilus. It is unlikely that the molecular substructures identified by STM were due to associated $c$-cytochromes because the beadlike electronic structures of the pilus imaged by STM had a diameter consistent with the diameter of the pilus shaft and an axial periodicity (7–8 nm) in the ranges reported for the periodicity of the major groove of type IV pili [15]. Furthermore, these periodicities contrasted with the uneven association of cytochromes previously reported along pili-like filaments in *G. sulfurreducens* [5]. These similarities in electronic and structural periodicity suggest that the electronic structure resolved by STM was intrinsic to the pilus shaft.

We further characterized the pilus electronic properties by STM spectroscopy. For these experiments, the STM tip was placed above the pilus, as shown schematically in [Fig. 3(a)]. Figure 3(b) shows a representative $I$-$V$ (current versus voltage) measurement at biological ($\pm 1$ V) voltages and in reference to a HOPG control. The slope of the pilus $I$-$V$ curve is greater than zero, even near zero voltage (the Fermi level). Hence, the pili are conductive even at low voltages (millivolts), as previously reported [1]. Differential conductance $dI/dV$ as a

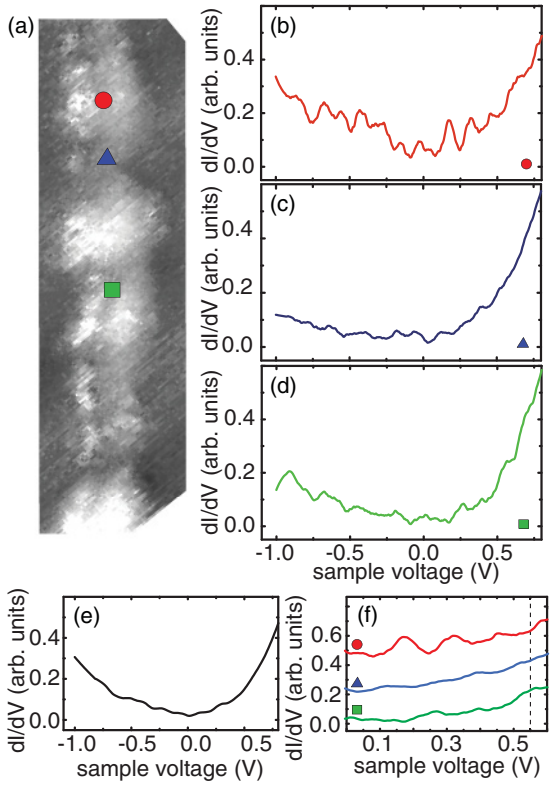


FIG. 4. (Color online) Differential conductance $dI/dV$ spectra obtained with the tip placed above three different points on the pilus shown in the left panel. The color and sequence of each point located in the image (a) matches the color and sequence of the $dI/dV$ curves (b)–(d). Each $dI/dV$ curve (b)–(d) is the numerical derivative of the average of 1000 consecutive $I$-$V$ curves. Curves were filtered with 29-point Savitzky-Golay smoothing before and after differentiation. (e) $dI/dV$ curve taken on the graphite substrate $\sim$50 nm away from the pilus. This curve was processed with an additional filtering step of 75-point Savitzky-Golay smoothing. (f) Subset of pilus curves (b)–(d) in the voltage range that contains cytochrome hemes signatures [9].

function of voltage $V$ at various locations on the pilus filament [Fig. 4(a)] showed a reproducible asymmetric structure with respect to the voltage polarity [Figs. 4(b)–4(d)], which contrasted with the more symmetric graphite conductance curve [Fig. 4(e)]. Conductance asymmetry has previously been reported in protein assemblies of helical subunits and has been linked to the dipolar nature of proteins, which contain a carboxy- and an amino-terminus ends [16]. Although the pilus $dI/dV$ curves contained peaks suggestive of discrete energy levels, many of these features were not reproducible. Thus, they do not correspond to intrinsic electronic features of the pilus and are likely due to noise. Of special significance was the absence of a peak feature at ∼0.55 V in all the curves [Fig. 4(f)], which has been proposed to arise from the contribution of electronic energy levels of the heme group from cytochromes [17]. This contrasts with the distinct and reproducible peaks of the cytochrome-containing nanowires produced by *S. oneidensis*, which consistently show a prominent peak at ∼0.55 V linked to the presence of the MtrC cytochrome [9].

In conclusion, despite the challenges associated with probing heterogeneous biological samples by STM, we successfully imaged and characterized the transversal conductive properties of cell-associated, untreated pili, thus ruling out any artifacts derived from cell-free preparations enriched in pili and other outer membrane components [1] and from the use of chemical [5] or physical [6] treatments. Our STM data did not show features that could reflect a contribution of cytochrome heme groups but, rather, were consistent with topographic and electronic features intrinsic to the pilus shaft. This suggests that the pilus shaft plays a direct role in electron transfer. This is significant because the conductive pili produced by *Geobacter* bacteria are formed through the assembly of a single peptide subunit [4], a process that could be harnessed for the development of protein nanowires and biocompatible nanostructured devices.

The authors would like to thank Blair Bullard and Catherine Silva for assistance with the preparation of biological samples and CSLM analyses. AFM work was performed in the Keck Microfabrication Facility at MSU. This work was supported by Grant No, R01-ES017052-03 from the NIEHS Superfund Program, Grant No. MCB 1021948 from NSF, and a Strategic Partnership Grant from the Michigan State University Foundation.

[1] G. Reguera, K. D. McCarthy, T. Mehta, J. S. Nicoll, M. T. Tuominen, and D. R. Lovley, Nature (London) **435**, 1098 (2005).

[2] G. Reguera, R. B. Pollina, J. S. Nicoll, and D. R. Lovley, J. Bacteriol. **189**, 2125 (2007).

[3] G. Reguera, K. P. Nevin, J. S. Nicoll, S. F. Covalla, T. L. Woodard, and D. R. Lovley, Appl. Environ. Microbiol. **72**, 7345 (2006).

[4] D. L. Cologgi, S. Lampa-Pastirk, A. M. Speers, S. D. Kelly, and G. Reguera, Proc. Natl. Acad. Sci. USA **108**, 15248 (2011).

[5] C. Leang, X. Qian, T. Mester, and D. R. Lovley, Appl. Environ. Microbiol. **76**, 4080 (2010).

[6] N. S. Malvankar *et al.*, Nat. Nanotechnol. **6**, 573 (2011).

[7] M. Y. El-Naggar, G. Wanger, K. M. Leung, T. D. Yuzvinsky, G. Southam, J. Yang, W. M. Lau, K. H. Nealson, and Y. A. Gorby, Proc. Natl. Acad. Sci. USA **107**, 18127 (2010).

[8] Y. A. Gorby *et al.*, Proc. Natl. Acad. Sci. USA **103**, 11358 (2006).

[9] M. Y. El-Naggar, Y. A. Gorby, W. Xia, and K. H Nealson, Biophys. J. **95**, L10 (2008).

[10] C. Baldacchini and S. Cannistraro, J. Nanosci. Nanotechnol. **10**, 2753 (2010).

[11] T. Mehta, M. V. Coppi, S. E. Childers, and D. R. Lovley, Appl. Environ. Microbiol. **71**, 8634 (2005).

[12] K. Besocke, Surf. Sci. **181**, 145 (1987).

[13] S. H. Tessmer, D. J. Van Harlingen, and J. W. Lyding, Rev. Sci. Instrum. **65**, 2855 (1994).

[14] L. P. Biró, J. Gyulai, Ph. Lambin, J. B. Nagy, S. Lazarescu, G. I. Mark, A. Fonseca, P. R. Surján, Zs. Szekeres, P. A. Thiry, and A. A. Lucas, Carbon **36**, 689 (1998).

[15] L. Craig, N. Volkmann, A. S. Arvai, M. E. Pique, M. Yeager, E. H. Egelman, and J. A. Tainer, Molec. Cell **23**, 651 (2006).

[16] P. K. Kienker, W. F. DeGrado, and J. D. Lear, Proc. Natl. Acad. Sci. USA **91**, 4859 (1994).

[17] N. S. Wigginton, K. M. Rosso, and M. F. Hochella, J. Phys. Chem. B **111**, 12857 (2007).